


---

**Proceedings Paper:**
Hua, H., Zhu, Z.Q. orcid.org/0000-0001-7175-3307, Pride, A. et al. (2 more authors) (2017) Comparative study of variable flux memory machines with parallel and series hybrid magnets. In: 2017 IEEE Energy Conversion Congress and Exposition (ECCE). 2017 IEEE Energy Conversion Congress and Exposition (ECCE), 01-05 Oct 2017, Cincinnati, OH, USA. IEEE , pp. 3942-3949. ISBN 9781509029983

https://doi.org/10.1109/ECCE.2017.8096691

---

# Comparative Study on Variable Flux Memory Machines with Parallel or Series Hybrid Magnets

Hao Hua, Z.Q. Zhu
Department of Electronics and Electrical Engineering
University of Sheffield, Sheffield, S1 3JD, U.K.

Adam Pride, Rajesh Deodhar, Toshinori Sasaki
IMRA Europe S.A.S. U.K. Research Center
Brighton, BN1 9RS, U.K.

***Abstract*—Variable flux memory (VFM) permanent magnet (PM) machines exhibit an additional degree-of-freedom for control, i.e. PM magnetization state, and thus excellent flux controllability. Moreover, the hybrid PM topologies having variable PM (VPM) with low coercive force and constant PM (CPM) with high coercive force at the same time, are employed to improve the torque density and the flux controllability. The parallel and series connections between the two different kinds of PMs are both feasible. Based on equivalent magnetic circuits, two-dimensional (2-D) finite element (FE) analyses and experiments, the VFM machines with these two connection types are investigated and compared in this paper. The results reveal that the VPM with series connected CPM is beneficial for more stable working point and higher torque density. A pair of VFM prototypes with parallel and series hybrid PMs respectively are manufactured and tested to validate the analyses.**

***Keywords—magnetization; memory machine; parallel hybrid; permanent magnet; series hybrid; variable flux***

## I. Introduction

Although permanent magnet (PM) machines benefit from high efficiency and high torque density, the relatively fixed magnetic field of PMs brings challenges to effective and efficient flux-weakening during high-speed operations [1], [2], which is important in variable-speed applications. Based on the vector control principle, a negative *d*-axis armature current ($-I_d$) can be applied to counter the PM flux and thus to realize flux-weakening, which is currently a popular solution in the PM machine-based variable-speed applications [3]. However, the overall armature current capacity and/or power capability may be limited, whilst the extra copper loss continuously exists and hence the efficiency is sacrificed.

Consequently, the variable flux memory (VFM) machines employing variable PMs (VPMs), i.e. PMs with low coercive force, have been proposed [4], [5]. The essential feature of the VFM machines is that the magnetization state of the PMs can be varied by a current pulse and then is memorized after the current is released. As a result, the VFM machines exhibit excellent flux controllability whilst dissipating negligible extra copper loss. The PM magnetization state can be flexibly regulated to match various operation conditions, in which the flux-weakening is easily achieved and the high efficiency is maintained. A multitude of VFM topologies by replacing the constant PMs (CPMs), e.g. NdFeB, in the conventional PM machines, with the VPMs, have been investigated in the past decade. In [6]-[8], the VFM concept has been applied to the flux-intensifying interior-PM (IPM) machines, whose *d*-axis inductance ($L_d$) exceeds *q*-axis inductance ($L_q$) by adopting *q*-axis flux barriers in the rotor. Consequently, the positive reluctance torque is obtained with $+I_d$ whilst the VPM magnetization state is stabilized simultaneously. Moreover, the spoke-type IPM rotor can be employed to boost the PM usage volume and hence the torque output [9]-[11]. In addition, the VFM concept can also be applied to the stator-PM machines, in which the VPMs are allocated on the stators to obtain a robust rotor topology [12], [13]. Nevertheless, since the relatively weak VPMs are solely employed, the torque densities of these VFM machines are always lower than the counterparts equipped with CPMs.

Therefore, the hybrid PM configurations are proposed to boost the torque density of the VFM machines, where the CPMs provide a constant field and the VPMs offer an additional variable component [14]. The two kinds of PMs can be magnetically connected in either series or parallel. Therefore, the advantages of high torque density in the conventional PM machines and the synergies of good flux controllability in the VFM machines are combined together. In [14]-[19], the VPM and CPM are located on the same rotor pole, and the CPM flux tends to bypass the VPM. Hence, the total amount of the effective flux equals to the sum of the flux generated by CPM and VPM, i.e. the parallel connection between the two different kinds of PMs is presented. However, the working point of the VPM is unstable and may be automatically demagnetized by the adjacent CPM itself. In [15], [20]-[23], the VFM machines with series connections between CPMs and VPMs are proposed, where the CPM flux would flow through the VPM and thus assist it to stabilize the working point. The CPM and VPM can be placed on the same pole, in which they are jointed together to have a series connection [15], [20]. Alternatively, the VPM and CPM can be alternately mounted on the every two adjacent rotor poles, where all VPMs are magnetized with the identical polarity while all CPMs have the opposite identical polarity [21]-[23].

In this paper, based on the commercial Toyota Prius2010 IPM machine dimensions and the common flux-weakening salient IPM topology, a pair of VFM machines employing parallel and series hybrid PMs are compared to identify their

different features, which could offer a guideline for the design and analysis of VFM traction machines [24].

The paper is organized as follows. In section II, the topologies and operating principle of the two VFM machines are briefly described, followed by the investigation on their equivalent magnetic circuits in section III. Afterwards, in section IV, the electromagnetic performances of the parallel and series hybrid VFM machines are evaluated based on two-dimensional (2-D) finite element (FE) method. The characteristics of variable back-EMF, torque capability, demagnetization and re-magnetization, and torque-speed envelope are comprehensively compared. In section V, a pair of VFM prototypes with parallel and series hybrid PMs respectively, are manufactured and tested for experimental verification. Finally, in section VI, the essential advantages of VFM machines, i.e. the efficiency performance of the two machines are illustrated.

## II. Machine Topology and Operating Principle

The cross sections of the parallel and series hybrid VFM machines are shown in Figs. 1(a) and (b) respectively, and their key design parameters are listed in Table I. The overall dimensions of the two machines are the same. In addition, the identical 48-stator-slot/8-rotor-pole structure and the identical distributed armature windings are inherited from the Prius2010 IPM machine, whilst the V-shaped IPM rotor topology is employed as well. The NdFeB and SmCo materials are used for CPM and VPM respectively. The PM thickness and flux barriers are optimized for the two machines for compromising the torque and flux regulation performance. In the parallel hybrid VFM machine, Fig. 1(a), two pieces of CPMs are located on each rotor pole and they are adjacent to the *d*-axis position, meanwhile, another two pieces of VPMs are placed at the side of the CPMs, and they are close to the *q*-axis position. A large number of flux barriers are applied on the rotor to alleviate the cross-coupling and help to maintain the working point of VPMs [6]-[11], [13]-[15]. In fact, these flux barriers are generally necessary in the sole VPM or parallel hybrid VFM machines for resisting the unintentional demagnetization. In contrast, the configuration of the series hybrid VFM machine is relatively simple, Fig. 1(b), which is similar to the conventional IPM machine but has CPMs and VPMs alternately placed on every two adjacent poles. As a result, all VPMs have the same polarity while all CPMs have the opposite one. The complicated rotor flux barriers are avoided since the VPM working point is inherently stable thanks to the assistance of CPMs.

The arrows in Fig. 1 indicate the magnetization polarities of PMs, and the polarities of VPMs can be adjusted in the two VFM machines (Figs. 1(a) and (c) for parallel hybrid machine whilst Figs. 1(b) and (d) for series hybrid machine). The variable flux principle can be explained with the major hysteresis loop of the employed VPM, Fig. 2(a), where the VPM working points under open-circuit condition are illustrated. It can be seen that the VPM has a relatively low coercive force ($H_c$), and its knee point, the point beyond which the demagnetization curve becomes nonlinear, is high in Quadrant II. Hence, the magnetization state of the VPM is easy to vary. For instance, if a high negative magneto-motive force (MMF) has been applied to push the VPM working point from the initial point *A* to the point *B* that is lower than the knee point, it would recover along the recoil line *BD* and terminate at point *C* after the MMF is released. Consequently, the intentional demagnetization is completed, and the corresponding new remanent flux density ($B_{rk}$) is lower than the original one ($B_r$). A magnetization ratio factor $k_m$ can be introduced to illustrate the resultant state of the VPM:

$$k_m = \frac{B_{rk}}{B_r} \quad (1).$$

Subsequently, if a high positive MMF is applied and then released, the VPM working point could shift to point *F* along the curve *CDEF*, which corresponds to another remanent flux density. Therefore, the VPM magnetization state is flexibly regulated, resulting in the variable flux in the VFM machine. In contrast, the demagnetization curve of CPM is linear in Quadrant II, Fig. 2(b), and thus it is difficult to vary the remanent flux density.

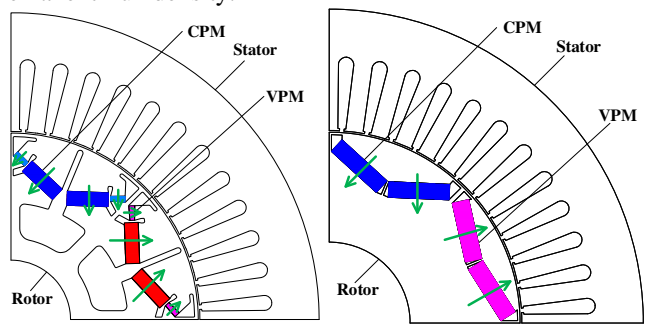


(a) Parallel hybrid with forward magnetized VPM

(b) Series hybrid with forward magnetized VPM

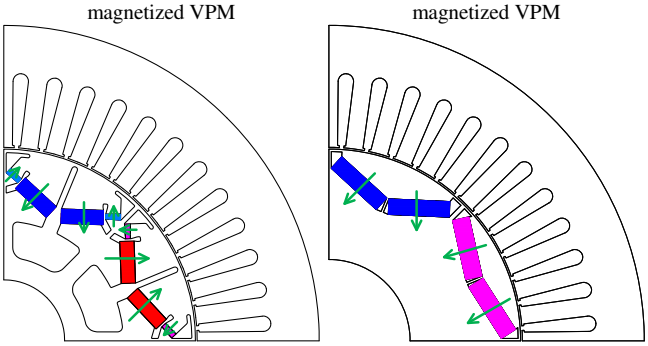

(c) Parallel hybrid with reverse magnetized VPM

(d) Series hybrid with reverse magnetized VPM

Fig. 1 Cross sections of parallel and series hybrid VFM machines.

TABLE I.
KEY DESIGN PARAMETERS OF PARALLEL AND SERIES VFM MACHINES.

| Parameter | Series hybrid | Parallel hybrid |
|---|---|---|
| Phase number | 3 | 3 |
| Stator slot/rotor pole number | 48/8 | 48/8 |
| Axial length (mm) | 50.8 | 50.8 |
| Stator outer diameter (mm) | 264 | 264 |
| Stator inner diameter (mm) | 161.9 | 161.9 |
| Rotor outer diameter (mm) | 160.44 | 160.44 |
| Rotor inner diameter (mm) | 68 | 68 |
| Air-gap length (mm) | 0.73 | 0.73 |
| CPM thickness (mm) | 6.5 | 6 |
| CPM width (mm) | 25 | 17.6 |
| VPM thickness (mm) | 7 | 2-2.5 |
| VPM width (mm) | 25 | 6.3 |
| CPM $B_r$ (T) | 1.2 | 1.2 |
| CPM $H_c$ (kA/m) | 915 | 915 |
| VPM $B_r$ (T) | 1.14 | 1.14 |
| VPM $H_c$ (kA/m) | 335 | 335 |
| Steel grade | 35H270 | 35H270 |
| Number of turns per coil | 11 | 11 |
| Number of coils per phase | 8 | 8 |
| Rated current density (A/mm$^2$) | 26.8 | 26.8 |

The working point of VPM would be slightly different in the hybrid PM VFM machines, due to the functions of CPMs. Since the VPMs and CPMs are placed in parallel in the parallel hybrid machines, the CPM flux has the potential to short-circuit through the VPM and thus counter against the VPM. As a result, the open-circuit working points of VPM would be pushed downward, i.e. from points $A$, $C$, $F$ to points $A_p$, $C_p$, $F_p$ respectively, Fig. 2(a). Consequently, the VPM working points with parallel hybrid connection would be lower than those without CPM, indicating easier demagnetization. On the other hand, in the series hybrid machines, the CPM flux would flow forward through the VPM and hence assist it to stabilize the working point. Therefore, the VPM working points are pushed positively to $A_s$, $C_s$, $F_s$, respectively, Fig. 2(a), i.e. the flux density in the VPM is enhanced by the CPM and the work points become more stable.

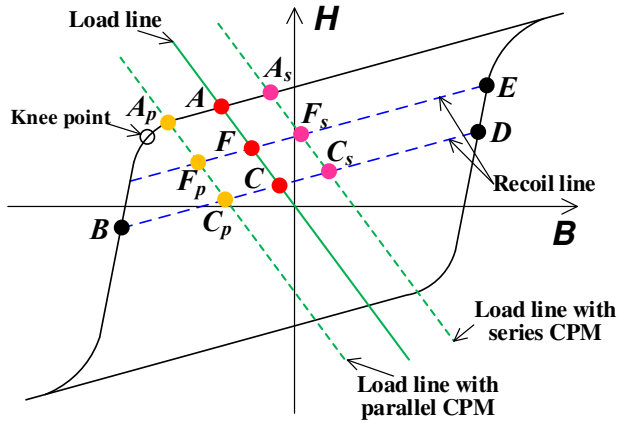


(a) VPM

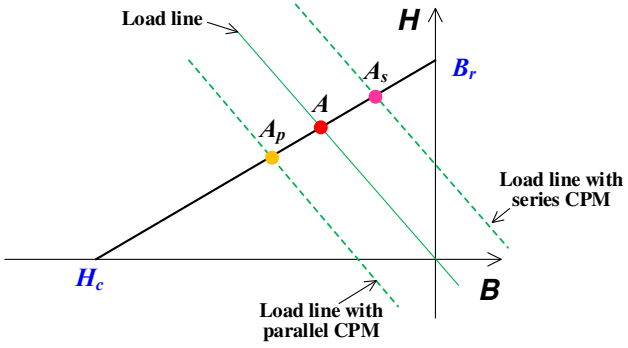


(b) CPM

Fig. 2 Illustration of working point of PM in open-circuit condition (B: flux density, H: magnetic field strength).

## III. Equivalent Magnetic Circuits

In order to better illustrate the features of the parallel and series hybrid PMs, their equivalent magnetic circuits are demonstrated in Figs. 3(a) and (b) respectively. $F_1$ ($F_2$), $R_{m1}$ ($R_{m2}$) represent the intrinsic MMF and the reluctance of CPM (VPM), whilst $R_g$ is the equivalent air-gap reluctance.

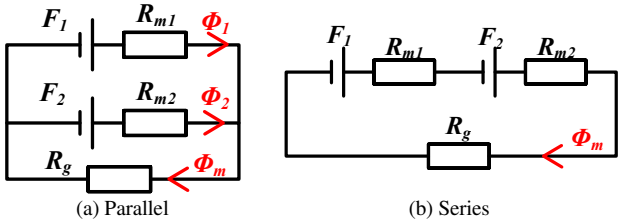


(a) Parallel (b) Series

Fig. 3 Illustration of parallel and series flux paths.

In the parallel circuit, the main flux through air-gap ($\Phi_{m\_p}$) is equal to the sum of the two parallel branches, i.e. the sum of the CPM flux ($\Phi_1$) and VPM flux ($\Phi_2$). According to the basic principle, the corresponding flux can be expressed as follows:

$$\Phi_{m\_p} = \Phi_1 + \Phi_2 \tag{2}$$

$$\Phi_1 = \frac{R_{m1}}{R_{m1} + R_{m2}//R_g} \cdot \frac{F_1}{R_{m1}} - \frac{R_{m1}//R_g}{R_{m1}//R_g + R_{m2}} \cdot \frac{F_2}{R_{m1}} \tag{3}$$

$$\Phi_2 = \frac{R_{m2}}{R_{m2} + R_{m1}//R_g} \cdot \frac{F_2}{R_{m2}} - \frac{R_{m2}//R_g}{R_{m2}//R_g + R_{m1}} \cdot \frac{F_1}{R_{m2}} \tag{4}.$$

It should be noted that the VPM flux ($\Phi_2$) may be negative if the VPM MMF ($F_2$) is remarkably low, which implies that the CPM flux may flow against the VPM. Therefore, the CPM flux potentially short-circuits via the VPM branch, and it actually can demagnetize the VPM if the two branches are not balanced. Therefore, the cross-coupling between the CPM and the VPM is severe in the parallel hybrid configuration, which unstabilises the working point of the VPM [14]. Moreover, the intrinsic MMF and reluctance of PM can be expressed by the PM dimensions and properties:

$$R_{m1} = \frac{t_1}{\mu_{r1}\mu_0 A_1} \tag{5}$$

$$R_{m2} = \frac{t_2}{\mu_{r2}\mu_0 A_2} \tag{6}$$

$$F_1 = H_{c1}t_1 = \frac{B_{r1}t_1}{\mu_{r1}\mu_0} \tag{7}$$

$$F_2 = H_{c2}t_2 = \frac{k_m B_{r2}t_2}{\mu_{r2}\mu_0} \tag{8}$$

where $t_1$ ($t_2$), $A_1$ ($A_2$), $B_{r1}$ ($B_{r2}$), $H_{c1}$ ($H_{c2}$), $\mu_{r1}$ ($\mu_{r2}$) are the thickness, cross section area perpendicular to magnetization direction, remanent flux density, coercive force and relative permeability of CPM (VPM) respectively, and $\mu_0$ is the magnetic permeability of air.

By substituting (3)-(8) into (2), the main flux through the air-gap in the parallel hybrid PMs is:

$$\Phi_{m\_p} = \frac{B_{r1}A_1 + k_m B_{r2}A_2}{1 + R_g\mu_0 A_1 A_2 (A_1 t_2 \mu_{r1} + A_2 t_1 \mu_{r2})/(t_1 t_2)} \tag{9}.$$

On the other hand, there is only one magnetic path in the series hybrid circuit and the CPM flux always flows forward through the VPM. Hence, the CPM naturally assists the VPM to withstand the unintentional demagnetization. The main flux flowing through the two kinds of PMs can be expressed as:

$$\Phi_{m\_s} = \frac{F_1 + F_2}{R_{m1} + R_{m2} + R_g} \tag{10}.$$

By substituting (5)-(8) into (10), it yields:

$$\Phi_{m\_s} = \frac{A_1 A_2 (\mu_{r2} B_{r1} t_1 + k_m \mu_{r1} B_{r2} t_2)}{\mu_{r2} A_2 t_1 + \mu_{r1} A_1 t_2 + R_g \mu_0 \mu_{r1} \mu_{r2} A_1 A_2} \tag{11}.$$

According to (9) and (11), it is clear that the resultant PM flux can be regulated in the parallel and series hybrid VFM machines, by changing the VPM magnetization state, i.e. adjusting $k_m$. In addition, it can be found that the working point of the VPM in the series hybrid configuration is more stable than that in the parallel counterpart.

## IV. Electromagnetic Performance Comparison

Based on 2-D FE method, the electromagnetic performances of the parallel and series hybrid VFM machines are comprehensively compared in this section.

### *A. Open-circuit field distributions*

Fig. 4 shows their open-circuit field distributions in the two typical magnetization states, i.e. VPM fully forward magnetized ($k_m$= 1) in Figs. 4(a) and (c), and VPM fully reverse magnetized ($k_m$= -1) in Figs. 4(b) and (d). In the parallel hybrid machine, it can be seen that the CPM contributes to an air-gap field together with the forward magnetized VPM, Fig. 4(a). Alternatively, the CPM flux short-circuits through the VPM and the resultant air-gap field is significantly reduced when the VPM is reverse magnetized, Fig. 4(b). In the series hybrid machine, the CPM flux easily flows through the VPM and contributes to a strong air-gap field with VPM forward magnetized, Fig. 4(c). However, when the VPM is reverse magnetized, the alternately arranged CPM and VPM poles have the identical polarity in this series hybrid machine. Although the strong CPM still guarantees the polarity of the rotor field, the CPM flux has much more difficult to flow through the VPM and thus the resultant field is obviously weakened, Fig. 4(d).

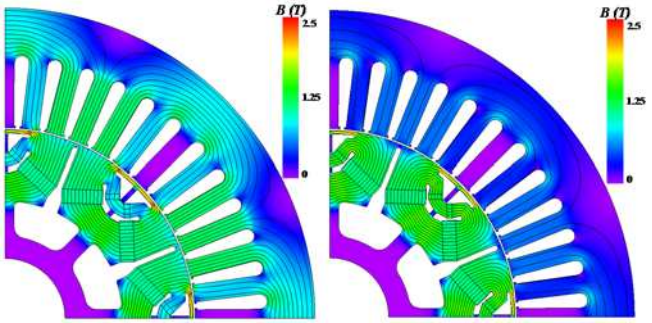

(a) Parallel hybrid with forward magnetized VPM ($k_m$=1)



(b) Parallel hybrid with reverse magnetized VPM ($k_m$= -1)

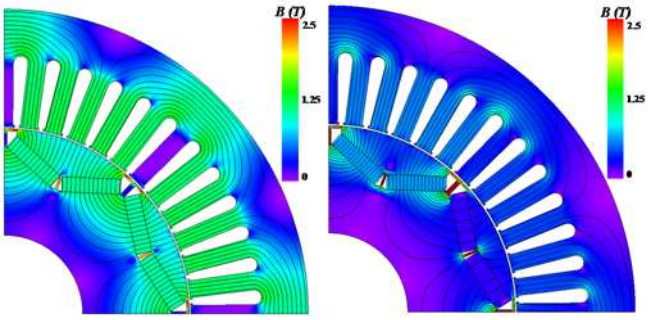

(c) Series hybrid with forward magnetized VPM ($k_m$=1)

(d) Series hybrid with reverse magnetized VPM ($k_m$= -1)

Fig. 4 Open-circuit field distributions in the two typical magnetization states.

The open-circuit radial flux densities in air-gap are compared in Fig. 5, where the significant differences between the forward and reverse magnetization states are observable in the two machines, which implies the wide flux variation ranges. The flux density amplitudes in the forward state are both remarkably higher than those in the reverse state. Meanwhile, it should be noted that the frequency of the air-gap flux densities is always constant and thus the rotor pole-pair number of both machines is unchanged in different states. Besides, the even order harmonics occur in the series hybrid VFM machine due to the rotor structure of alternate PMs, especially it is more significant in the reverse state. However, the even order harmonics will be cancelled out in the phase back-EMFs, which will be introduced in the following.

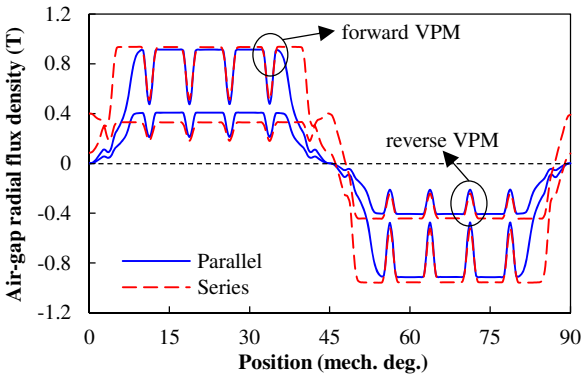


(a) Waveforms

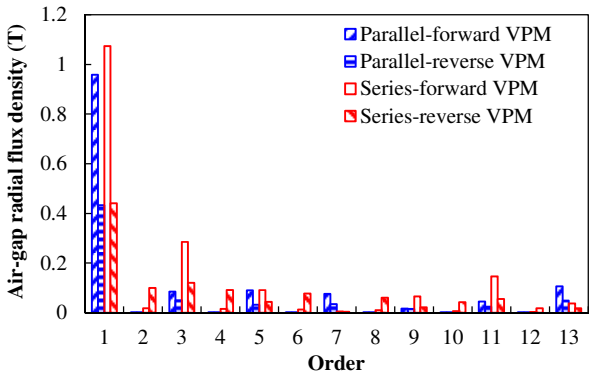


(b) Spectra

Fig. 5 Open-circuit air-gap radial flux densities in the two typical magnetization states.

### *B. Open-circuit back-EMF*

Fig. 6 compares the corresponding phase back-EMFs at 1500 r/min of the parallel and series hybrid VFM machines. It can be found that the even order harmonics are always absent in the two machines in both forward and reverse states. In fact, the even order spatial harmonics in the series hybrid VFM machine are cancelled out thanks to the winding configuration, with which the symmetrical phase back-EMFs free from the even order items are obtained. Moreover, the wide back-EMF variation ranges can be seen in both machines, which is 45%-100% in the parallel hybrid machine while 41%-100% in the series counterpart.

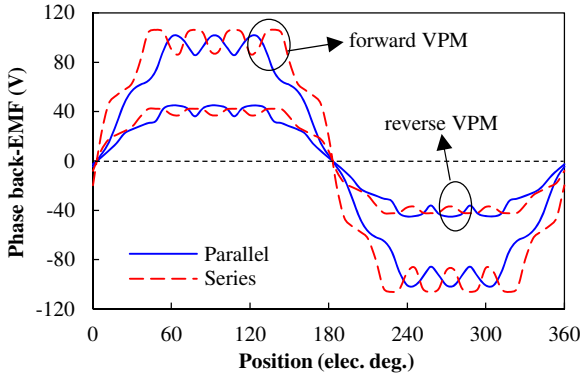


(a) Waveforms

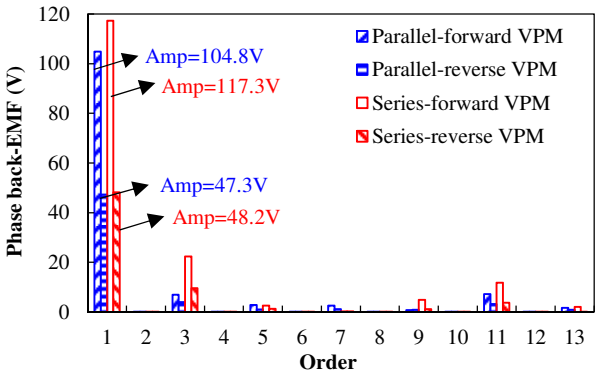


(b) Spectra

Fig. 6 Open-circuit phase back-EMFs at 1500 r/min in the two typical magnetization states.

### C. Torque capability

The torque capabilities of the parallel and series hybrid VFM machines are evaluated. The forward magnetization state is capable of exhibiting the highest torque output due to the high back-EMFs. Therefore, in the forward state, the average torques versus current angle (the phase angle between phase current and open-circuit back-EMF), with the rated current amplitude of 236A are compared in Fig. 7. Obviously, the reluctance torque is significant in the series hybrid machine but negligible in the parallel one. This can be explained by the fact that the rotor saliency ratio is sacrificed in the parallel hybrid VFM machine due to the sophisticated rotor flux barriers, whilst $-I_d$ component would greatly demagnetize the VPMs and weaken the PM field. In contrast, thanks to the better capability of resisting the unintentional demagnetization, the series hybrid VFM machine eliminates the complicated flux barriers and $-I_d$ component is acceptable during torque generation, with which the reluctance torque is re-obtained. As a consequence, the peak torque in the series hybrid machine is significantly higher than that of the parallel counterpart.

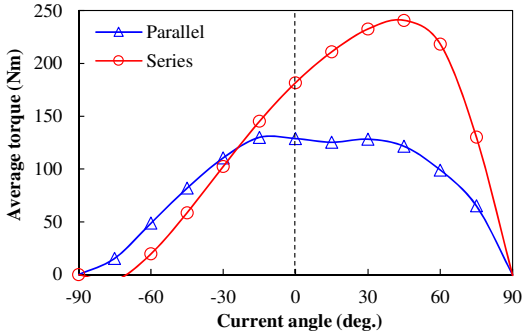


Fig. 7 Average torque versus current angle with fixed current amplitude of 236A in the full forward state.

The corresponding torque waveforms at the current angle of 0° and the current angle (45°) exhibiting reluctance torque are presented in Fig. 8. The cycle number of torque ripples during one electric period is always twelve in the two machines due to the identical slot/pole combinations. Furthermore, the average torques versus armature current amplitudes are illustrated in Fig. 9. With the fixed current angle of 0°, the series hybrid VFM machine always exhibits higher torque than the parallel one. Moreover, when the current angle is fixed at 45° to include the reluctance torque, the advantage of the series hybrid machine can be further enhanced.

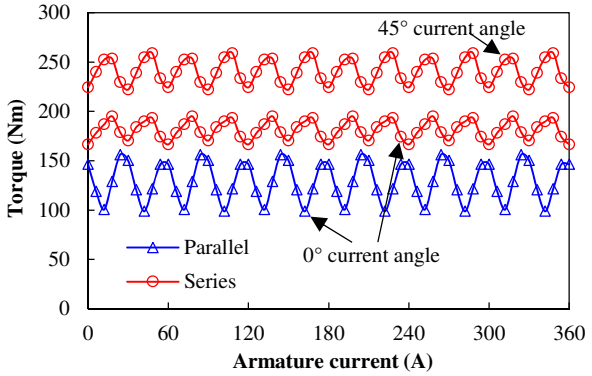


Fig. 8 Torque waveforms with current amplitude of 236A in the full forward state.

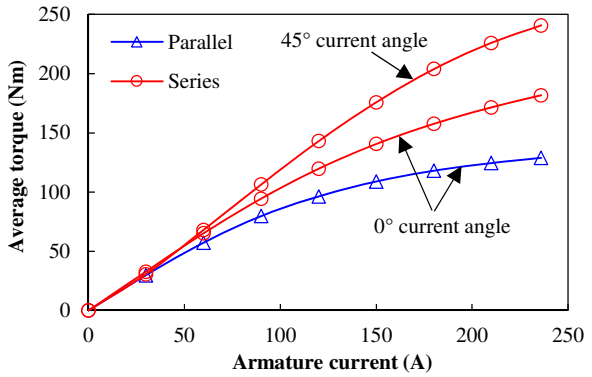


Fig. 9 Average torque versus current amplitude with fixed current angle of 0° or 45° in the full forward state.

### D. Unintentional demagnetization with $I_q$

The demagnetization due to $q$-axis current ($I_q$) is unfavourable in VFM machines, which would unintentionally degrade the machine performance [4], [5]. First of all, in order to investigate the CPM effects on the VPM in the two hybrid configurations, a monitoring line that, locates at the center of VPM and perpendicular to the magnetization direction, is employed. When the VPMs are non-magnetized ($k_m$=0), the flux densities along the magnetization direction on the monitoring line, due to the existence of CPMs, are evaluated in Fig. 10. It is clear that the VPM parallel connected to the CPM suffers the reversed flux and therefore tends to be demagnetized, while the series connected CPM provides the forward flux to the VPM and hence assists it in magnetizing. Moreover, based on the state with forward magnetized VPM, the unintentional demagnetization due to $I_q$ of the two machines are compared in Fig. 11, where the back-EMFs after different $I_q$ are presented. The back-EMF fundamental amplitudes decrease significantly in the parallel hybrid machine, implying that the VPMs have already been partially demagnetized. By comparison, there is only a negligible reduction of back-EMFs in the series hybrid machine, which reveals that the VPM working point is stable.

### E. Intentional demagnetization and re-magnetization with $I_d$

The intentional demagnetization and re-magnetization of VPMs are investigated, which is a challenge in VFM machines [6], [10], [15], [17]. The intentional demagnetization (with $-I_d$) based on the forward magnetized VPM state, and the re-magnetization (with $+I_d$) from the reverse magnetized VPM state, are illustrated in Fig. 12. The back-EMF fundamental amplitudes after different excitations are shown. The demagnetization is drastic in the parallel

hybrid machine and a low $-I_d$ can almost fully demagnetize the VPMs, as the CPMs naturally have the potential to help demagnetize the VPMs. In contrast, the back-EMFs decrease gradually in the series hybrid machine thanks to the assistance of the CPMs. Moreover, the re-magnetizations are always more challenging than the demagnetizations in the two machines due to the magnetic saturations. Although the re-magnetization of the VPM is facilitated by the CPM in the series hybrid VFM machine, a slightly higher current is required to realize the complete re-magnetization due to the relatively thick VPMs in the case.

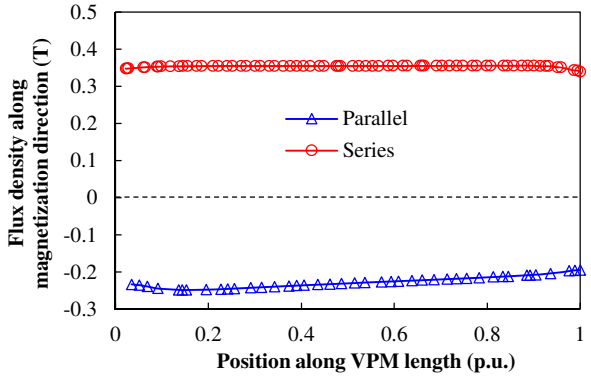


Fig. 10 Flux densities on monitoring line inside the VPM due to function of the CPM.

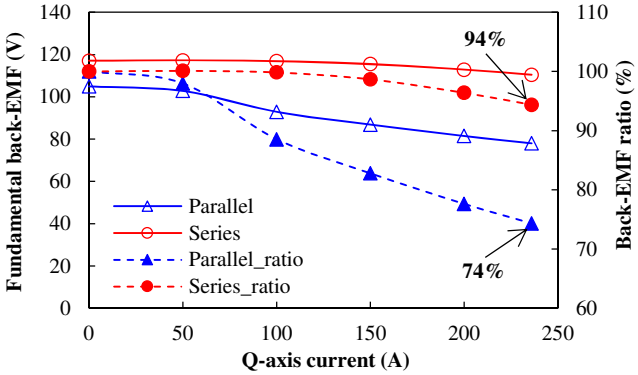


Fig. 11 Unintentional demagnetization due to $q$-axis current.

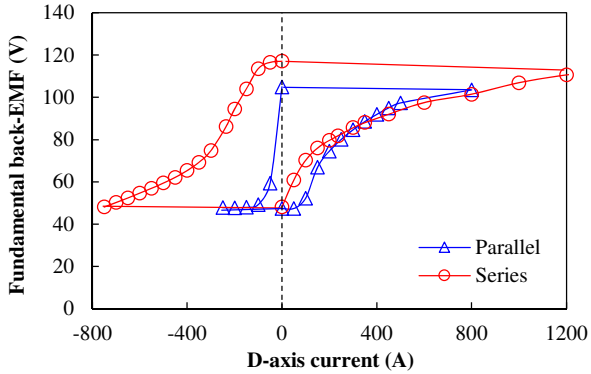


Fig. 12 Intentional demagnetization and re-magnetization due to $d$-axis current.

## F. Torque-speed envelop

Based on the flux-linkage method [25], the FE-predicted torque-speed and power-speed envelops are shown in Fig. 13. The flux-linkages of the machines excited with various current combinations are obtained from the sweep in FE simulations, and thus the output torque as well as the terminal voltage can be calculated. The full forward magnetization state is applied to the two machines, and the identical limits on bus voltage (650V) and phase current (236A) are employed. It can be observed that the parallel and series hybrid VFM machines both exhibit the wide constant power speed range (CPSR). Moreover, the series machine has remarkably higher torque than the parallel counterpart during low-speed range, which corresponds to the analysis in Figs. 7-9. The power output of the series machine is also higher in high-speed range.

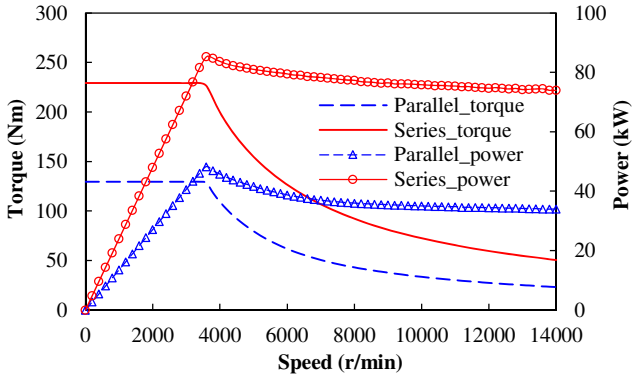


Fig. 13 Torque-speed and power-speed envelops in the full forward state.

## G. Efficiency characteristics

The major benefit of VFM machines is the reduction of continuous $-I_d$ during flux-weakening operation, which could benefit the machine efficiency [26], [27]. Therefore, it is essential to compare the efficiency performance of the two hybrid VFM machines. The efficiency map of the VFM machine is calculated, in which the iron losses and copper losses with different currents are swept based on FE method, and the optimum efficiency at each operation point is identified [28]. Since the magnetization state of the VPM will be regulated in the VFM machine to perform the appropriate PM flux, and thus, low copper loss and low iron loss are obtained, the different VPM magnetization states should be integrated together for the maximum efficiency. Therefore, the efficiency maps of the two VFM machines operating at different VPM magnetization states, including the full forward state ($k_m$= 1), non-magnetic state ($k_m$= 0) and full reverse state ($k_m$= -1) are all evaluated respectively. Fig. 14 (a)-(f) shows the efficiency maps of the two machines over the whole torque-speed envelops at different VPM magnetization states. It can be seen that the stronger VPMs contribute to not only higher torque output in the two machines but also higher efficiencies among the low-speed high-torque region. Alternatively, the weaker VPMs benefit from higher efficiencies among the high-speed region thanks to the reduction of $-I_d$ components. Meanwhile, it can be observed that the series hybrid machine exhibits remarkably higher torques and higher efficiencies during low-speed region than the parallel hybrid counterpart, while the parallel one has higher efficiencies during the high-speed operation.

Then, by integrating the efficiency maps of full forward and full reverse states for each machine, the integrated optimum efficiency performance is illustrated. Fig. 14 (g) and (h) illustrates the integrated efficiency maps of the parallel and series hybrid VFM machines respectively. In the two machines, the higher torque output is always obtained in the full forward state, and meanwhile, the efficiency is high in the low speed-high torque region. On the other hand, although the

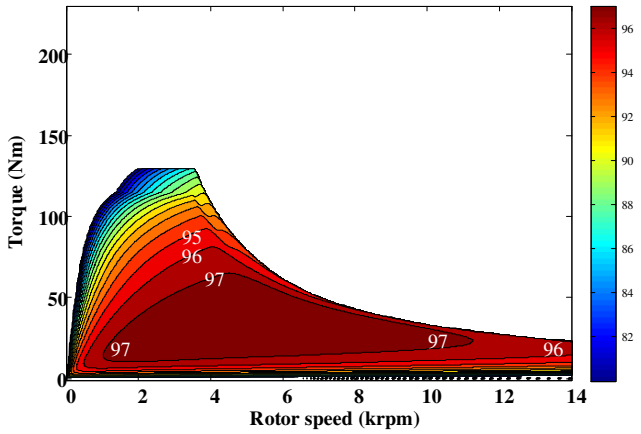


(a) Parallel hybrid, full forward VPM

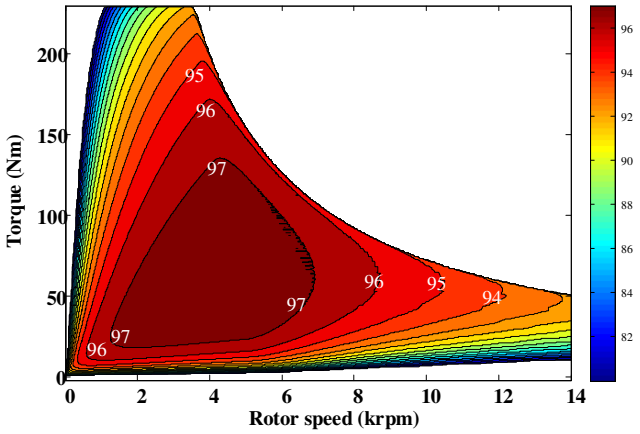


(b) Series hybrid, full forward VPM

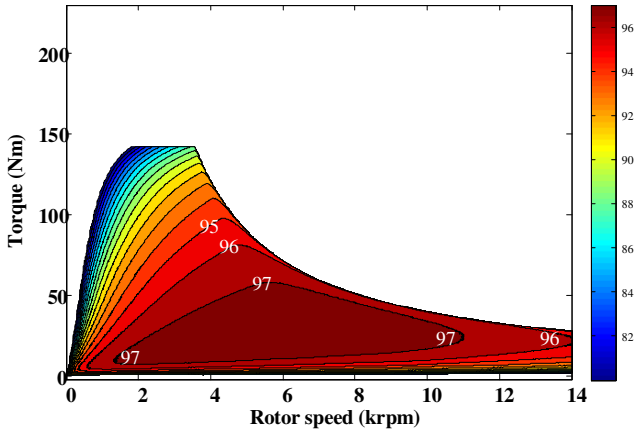


(c) Parallel hybrid, non-magnetic VPM

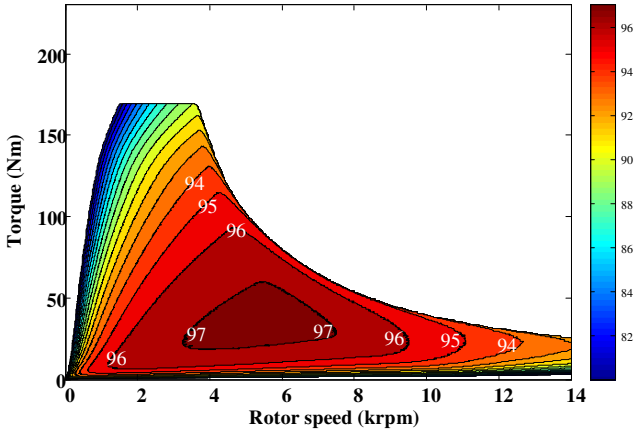


(d) Series hybrid, non-magnetic VPM

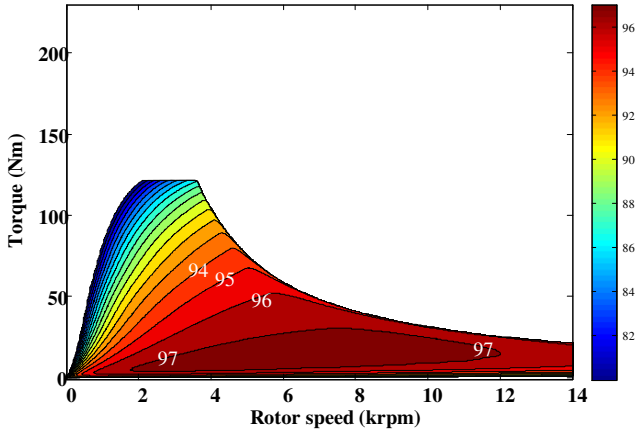


(e) Parallel hybrid, full reverse VPM

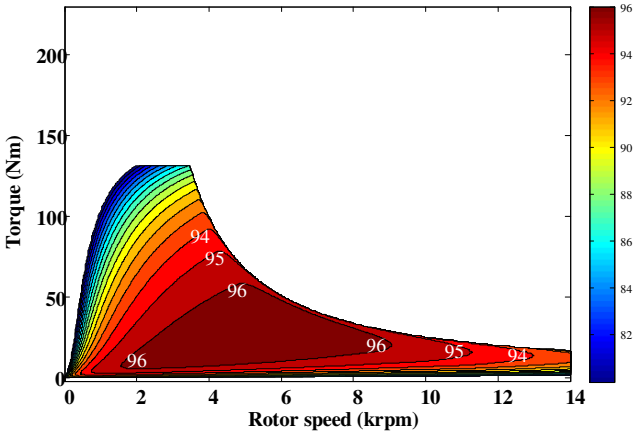


(f) Series hybrid, full reverse VPM

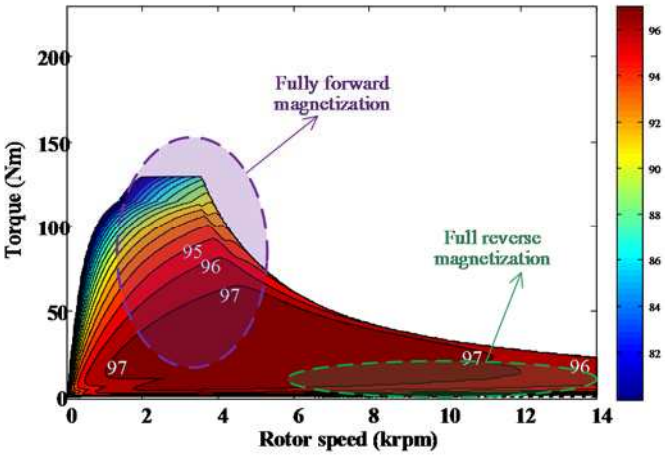


(g) Parallel hybrid, integrated full forward and full reverse states

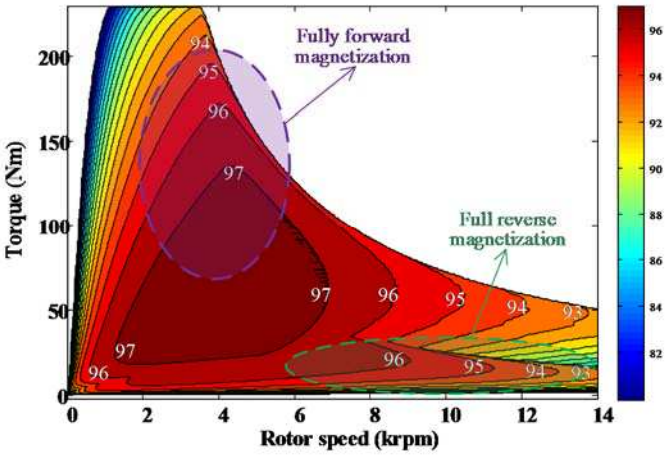


(h) Series hybrid, integrated full forward and full reverse states

Fig. 14 Integrated efficiency maps in the two typical magnetization states.

torque output is sacrificed in the full reverse state due to the weak PM, the efficiency in the high speed-low torque region can be significantly improved. Consequently, it is beneficial to flexibly switch the magnetization state at different operation regions, e.g. full magnetization during high torque region while partial magnetization during high speed region. By comparing the parallel and series hybrid VFM machines, it can be found that the series one has higher efficiency in the high torque operation, while the parallel one is advantageous in the high speed operation, albeit with lower power output.

## V. Experimental Validation

A pair of parallel and series hybrid VFM prototype machines, Fig. 15, are manufactured and tested to validate the predictions. The two machines share the stator and windings, and key design parameters of the prototypes are listed in Table I. The CPMs are fully magnetized while the VPMs are non-magnetized before fitting into the rotor. Based on the test platform shown in Fig. 16, $I_d$= +430A, which is the maximum available current of the inverter, is firstly applied to magnetize the VPMs. The open-circuit back-EMFs and on-load torques of the two prototypes in the maximum available magnetization states are measured, and the magnetization variations are also presented.

Fig. 17 shows the measured and 2-D, 3-D FE-predicted line back-EMFs at 1500 r/min in the maximum available magnetization state. Besides, in order to illustrate the flux variation of the prototypes, the back-EMF waveforms after different demagnetizing and re-magnetizing currents are shown in Figs. 18-19. In Fig. 18(a), the back-EMFs after positive *d*-axis currents are presented and the back-EMFs after demagnetization with negative *d*-axis currents are included in Fig. 18(b). The measured and 2D FE-predicted results are both presented. A significant variation range of the back-EMFs can be observed between these two figures. It can be found that the error between the measured and FE-predicted back-EMFs after re-magnetization is relatively high while that error after demagnetization is negligible. This is due to the fact that the demagnetization is easier than the re-magnetization in the parallel machine and a quite low current can fully demagnetize the VPMs. On the contrary, since the available current in the test platform is limited by the inverter and the VPMs cannot be fully re-magnetized, the working point of VPM would locate on the minor hysteresis loop, which is more challenging to accurately predict. Since the required re-magnetizing and demagnetizing currents are higher in the series hybrid VFM machine, the error due to the same reason can be easily seen in Figs. 19(a) and (b). Meanwhile, the end effect is more sever in the series machine due to the unbalanced rotor pole configurations [29], [30]. Furthermore, the rotor position sensitivity also contributes to the measurement error of the two machines as the precise *d*-axis current is expected in the test but the rotor may deviate a bit from the accurate position.

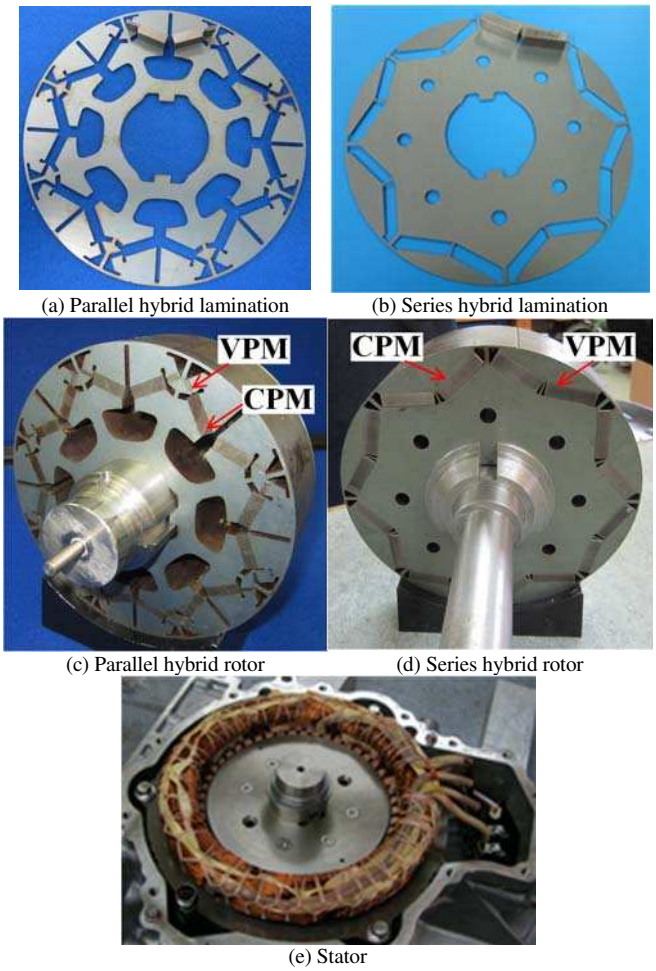


(a) Parallel hybrid lamination (b) Series hybrid lamination

(c) Parallel hybrid rotor (d) Series hybrid rotor

(e) Stator

Fig. 15 Prototypes of parallel and series hybrid VFM machines.

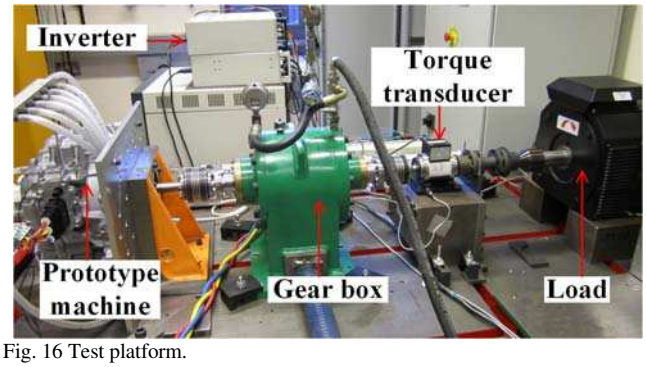


Fig. 16 Test platform.

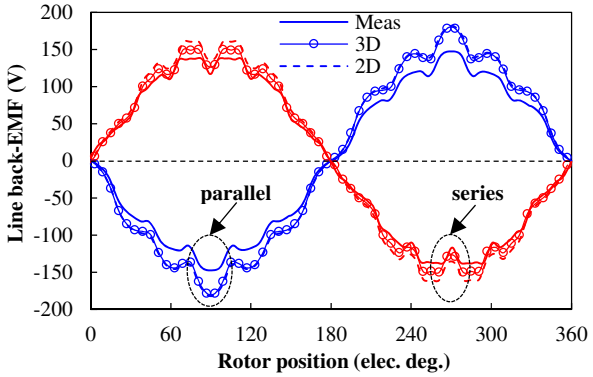


Fig. 17 FE-predicted and measured line back-EMFs at 1500 r/min in the maximum available magnetization state.

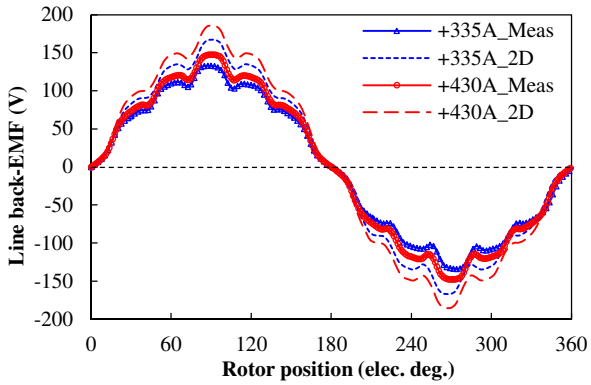


(a) Back-EMFs after re-magnetization

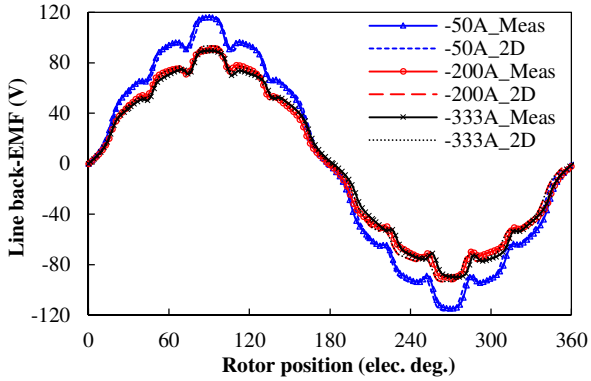


(b) Back-EMFs after demagnetization

Fig. 18 Measured and 2D FE-predicted line back-EMFs at 1500 r/min of the parallel hybrid VFM machine after various *d*-axis current excitations.

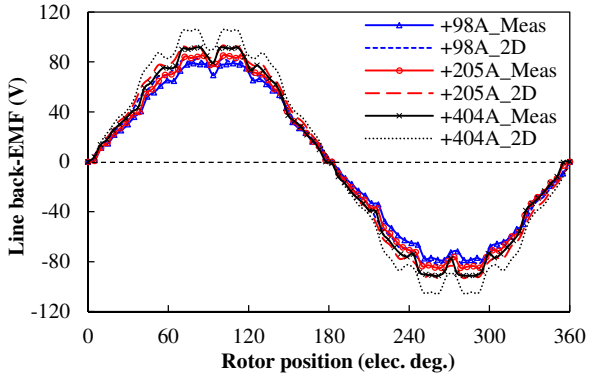


(a) Back-EMFs after re-magnetization

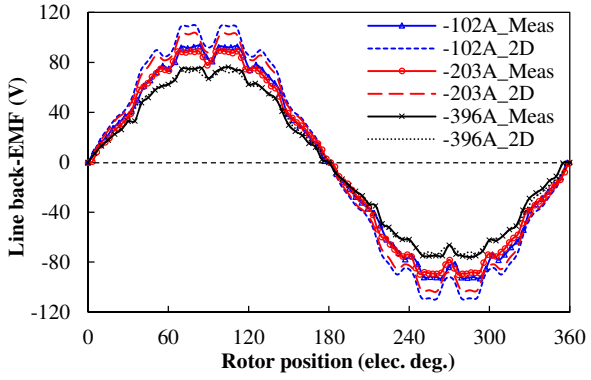


(b) Back-EMFs after demagnetization

Fig. 19 Measured and 2D FE-predicted line back-EMFs at 1500 r/min of the series hybrid VFM machine after various *d*-axis current excitations.

The torques of the two prototypes are also measured and shown in Figs. 20 and 21 respectively. Fig. 20 illustrates the measured and 2D FE-predicted torque waveforms with different *q*-axis currents of the parallel VFM machine. The measured and 2-D FE-predicted torque waveforms of the series machine are compared in Fig. 21(a), and quite significant difference between the predictions and test results is observed. In order to separate the severe end effect of the series hybrid VFM machine, the 3-D FE predictions are included in Fig. 21(b), which are more close to the measured results. Moreover, the variations of average torque versus $I_q$ are summarized in Fig. 22.

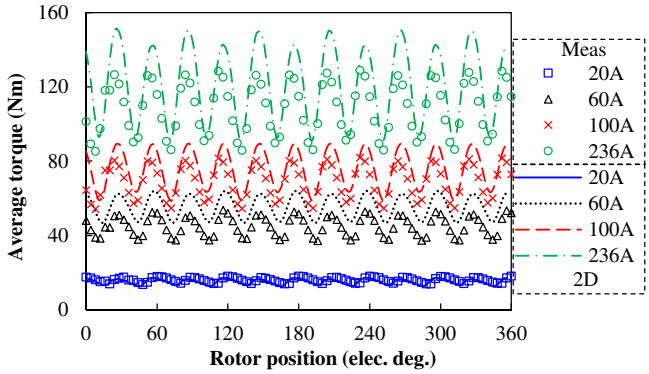


Fig. 20 Measured and 2D FE-predicted torque waveforms of the parallel hybrid VFM machine with various *q*-axis current in maximum available magnetization state.

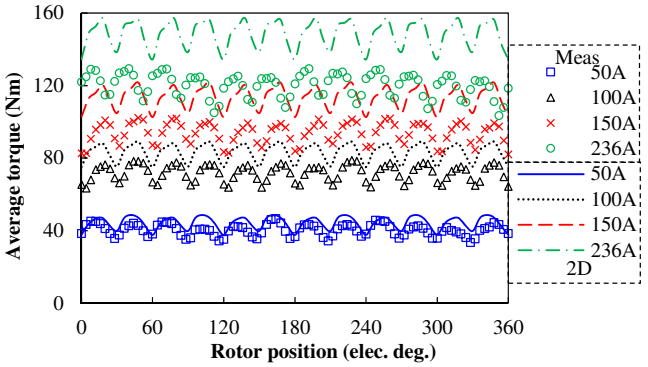


(a) Measured and 2D FE results

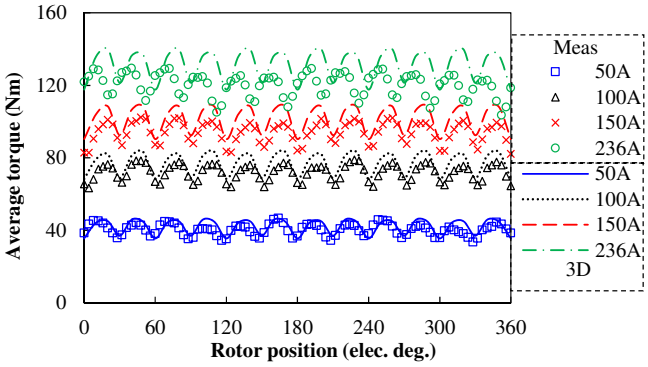


(b) Measured and 3D FE results

Fig. 21 Measured and FE-predicted torque waveforms of the series hybrid VFM machine with various *q*-axis current in maximum available magnetization state.

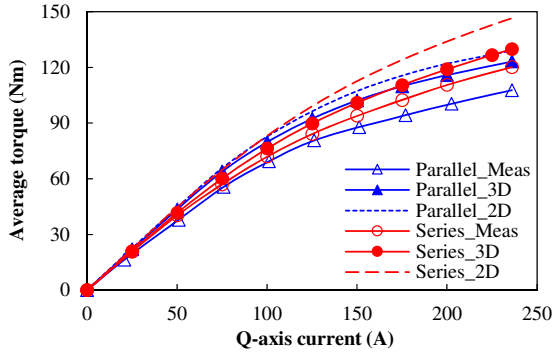


Fig. 22 Measured and FE-predicted average torques versus $I_q$ in maximum available magnetization state.

## VI. Conclusions

The parallel and series hybrid PM VFM machines based on the common IPM machine topology are investigated both theoretically and experimentally in this paper. According to the analysis on the equivalent magnetic circuits, the CPM effects on the VPM are identified in the two hybrid PM configurations. It is revealed that the parallel connected CPM potentially demagnetizes the VPM and hence the VPM working point is inherently instable. Alternatively, the VPM in the series hybrid PMs benefits from the assistance of the CPM and its working point is stable, with which the cross-coupling between the PMs is relieved. Therefore, the reluctance torque is re-obtained in the series hybrid VFM machine and the torque density is improved. However, the intentional demagnetization of the series hybrid VFM machine is also more challenging.

## References


[1] K.T. Chau, C.C. Chan, and C. Liu, "Overview of permanent-magnet brushless drives for electric and hybrid electric vehicles," *IEEE Trans. Ind. Electron.*, vol. 55, no. 6, pp. 2246-2257, Jun. 2008.

[2] Z.Q. Zhu and D. Howe, "Electrical machines and drives for electric, hybrid, and fuel cell vehicles," *Proc. IEEE*, vol. 95, no. 4, pp. 746-765, Apr. 2007.

[3] T.M. Jahns, G. Kliman, and T. Neumann, "Interior Permanent-magnet synchronous motors for adjustable-speed drives," *IEEE Trans. Ind. Appl.*, vol. IA-22, no. 4, pp. 738-747, Jul./Aug. 1986.

[4] V. Ostovic, "Memory motors-a new class of controllable flux PM machines for a true wide speed operation," in *Proc. Conf. Rec. IEEE – IAS Annu. Meeting*, 2001, pp. 2577–2584.

[5] V. Ostovic, "Memory motors," *IEEE Magn. Ind. Appl.*, vol. 9, no. 1, pp. 52-61, Jan./Feb. 2003.

[6] N. Limsuwan, T. Kato, K. Akatsu, and R.D. Lorenz, "Design and evaluation of a variable-flux flux-intensifying interior permanent magnet machine," in *Proc. Energy Convers. Cong. Expo. (ECCE)*, Sep. 2012, pp. 3670-3677.

[7] T. Kato, N. Limsuwan, C. Yu, K. Akatsu, and R.D. Lorenz, "Rare earth reduction using a novel variable magnetomotive force flux-intensified IPM machine," *IEEE Trans. Ind. Appl.*, vol. 50, no. 3, pp. 1748-1756, May/Jun. 2014.

[8] T. Fukushige, N. Limsuwan, T. Kato, K. Akatsu, and R.D. Lorenz, "Efficiency contours and loss minimization over a driving cycle of a variable-flux flux-intensifying interior machine," *IEEE Trans. Ind. Appl.*, vol. 51, no. 4, pp. 2984-2989, Jul./Aug. 2015.

[9] M. Ibrahim, L. Masisi, and P. Pillay, "Design of variable-flux permanent-magnet machines using Alnico magnets," *IEEE Trans. Ind Appl.*, vol. 51, no. 6, pp. 4482-4491, Nov./Dec. 2015.

[10] M. Ibrahim, L. Masisi, and P. Pillay, "Design of variable flux permanent-magnet machine for reduced inverter rating," *IEEE Trans. Ind. Appl*., vol. 51, no. 5, pp. 3666-3674, Sep./Oct. 2015.

[11] A. Sun, J. Li, R. Qu, J. Chen, and H. Lu, "Rotor design considerations for a variable-flux flux-intensifying interior permanent magnet machine with improved torque quality and reduced magnetization current," in *Proc. Energy Convers. Cong. Expo. (ECCE)*, Sep. 2015, pp. 784-790.

[12] C. Yu, K.T. Chau, X. Liu, and J.Z. Jiang, "A flux-mnemonic permanent magnet brushless motor for electric vehicles," *J. Appl. Phys.*, vol. 103, no. 07F103, 2008.

[13] X. Zhu, L. Quan, D. Chen, M. Cheng, Z. Wang, and W. Li, "Design and analysis of a new flux memory doubly salient motor capable of online flux control," *IEEE Trans. Magn.*, vol. 47, no. 10, pp. 3220-3223, Oct. 2011.

[14] Y. Chen, W. Pan, Y. Wang, R. Tang, and J. Wang, "Interior composite-rotor controllable-flux PMSM-memory motor," in *Proc. Inter. Conf. Elec. Mach. System. (ICEMS)*, Sep. 2005, vol. 1, pp. 446-449.

[15] K. Sakai, K. Yuki, Y. Hashiba, N. Takahashi, and K. Yasui, "Principle of the variable-magnetic-force memory motor," in *Proc. Inter. Conf. Elec. Mach. System. (ICEMS)*, Nov. 2009, pp. 1-6.

[16] D. Wu, Z.Q. Zhu, X. Liu, A. Pride, R. Deodhar, and T. Sasaki, "Cross coupling effect in hybrid magnet memory motor," in *Proc. Inter. Conf. Power Elec. Mach. and Drives (PEMD)*, Apr. 2014, pp. 1-6.

[17] Y. Zhou, Y. Chen, and J. X. Shen, "Analysis and improvement of a hybrid permanent magnet memory motor," *IEEE Trans. Energy Convers.*, vol. 31, no. 3, pp. 915-923, Sep. 2016.

[18] X. Liu, D. Wu, Z.Q. Zhu, A. Pride, R. Deodhar, and T. Sasaki, "Efficiency improvement of switched flux PM memory machine over interior PM machine for EV/HEV applications," *IEEE Trans. Magn.*, vol. 50, no. 11, pp. 8202104, Nov. 2014.

[19] H. Yang, H. Lin, Z.Q. Zhu, D. Wang, S. Fang, and Y. Huang, "A variable-flux hybrid-PM switched-flux memory machine for EV/HEV applications," *IEEE Trans. Ind. Appl.*, vol. 52, no. 3, pp. 2203-2214, May/Jun. 2016.

[20] A. Athavale, K. Sasaki, B. Gagas, T. Kato, and R. Lorenz, "Variable flux permanent magnet synchronous machine (VF-PMSM) design methdologies to meet electric vehicle traction requirements with reduced losses," *IEEE Trans. Ind. Appl.*, vol. 53, no. 5, pp. 4318-4326, Sep./Oct. 2017.

[21] S. Maekawa, K. Yuki, M. Matsushita, I. Nitta, Y. Hasegawa, and T. Shiga, "Study of the magnetization method suitable for fractional-slot concentrated-winding variable magnetomotive-force memory motor," *IEEE Trans. Power Electron.*, vol. 29, no. 9, pp. 4877-4887, Sep. 2014.

[22] J. Kim, J. Choi, K. Lee, and S. Lee, "Design and analysis of surface-mounted-type variable flux permanent magnet motor for wide-speed range applications," *IEEE Trans. Magn.*, vol. 51, no. 11, pp. 8111004, Nov. 2015.

[23] H. Hua, Z.Q. Zhu, A. Pride, R. Deodhar, and T. Sasaki, "A novel variable flux memory machine with series hybrid magnets," *IEEE Trans. Ind. Appl.*, vol. 53, no. 5, pp. 4396-4405, Sep./Oct. 2017.

[24] H. Hua, Z.Q. Zhu, A. Pride, R. Deodhar, and T. Sasaki, "Comparative study of variable flux memory machines with parallel and series hybrid magnets," in *Proc. Energy Convers. Cong. Expo. (ECCE)*, Oct. 1-5, 2017, pp. 1-8.

[25] G. Qi, J. Chen, Z.Q. Zhu, D. Howe, L. Zhou, and C. Gu, "Influence of skew and cross-coupling on flux-weakening performance of permanent-magnet brushless AC machines," *IEEE Trans. Magn.*, vol. 45, no. 5, pp. 2110-2117, May 2009.

[26] A. Aljehaimi, and P. Pillay, "Operating envelopes of the variable flux machine with positive reluctance torque," *IEEE Trans. Transport. Electrif.*, vol. 4, no. 3, pp. 707-719, Sep. 2018.

[27] A. Aljehaimi, and P. Pillay, "Torque and power improvement for a variable flux permanent magnet synchronous machine," in *Proc. Transport. Electrif. Conf. Expo (ITEC)*, Jun. 22-24, 2017, pp. 425-429.

[28] W. Chu, Z.Q. Zhu, J. Zhang, X. Liu, D. Stone, and M. Foster, "Investigation on operational envelops and efficiency maps of electrically excited machines for electrical vehicle applications," *IEEE Trans. Magn.*, vol. 51, no. 4, pp. 8103510, Apr. 2015.

[29] Z.Q. Zhu, H. Hua, A. Pride, R. Deodhar, and T. Sasaki, "Analysis and reduction of unipolar leakage flux in series hybrid permanent-magnet variable flux memory machines," *IEEE Trans. Magn.*, vol. 53, no. 11, pp. 2500604, May 2017.

[30] H. Hua, Z.Q. Zhu, A. Pride, R. Deodhar, and T. Sasaki, "Comparison of end effect in series and parallel hybrid permanent magnet variable flux memory machines," in *Proc. Inter. Conf. Elec. Mach. Sys. (ICEMS)*, Aug. 11-14, 2017, pp. 1-6.



**Hao Hua** was born in Hefei, China, in 1990. He received the M.Sc. degree from Southeast University, Nanjing, China, in 2014, and the Ph.D. degree at The University of Sheffield, Sheffield, U.K., in 2017, both in electrical engineering.

His current research interests include the design and analysis of permanent-magnet and hybrid-excited machines for applications in automotive and renewable energy. Dr. Hua was an award recipient at the IEEE Industry Applications Society Transactions Prize Paper of 2017.

**Z.Q. Zhu** (M'90–SM'00–F'09) received the B.Eng. and M.Sc. degrees in electrical and electronic engineering from Zhejiang University, Hangzhou, China, in 1982 and 1984, respectively, and the Ph.D. degree in electrical and electronic engineering from The University of Sheffield, Sheffield, U.K., in 1991.

Since 1988, he has been with the University of Sheffield, where since 2000, he has been a Professor with the Department of Electronic and Electrical Engineering. He is currently the Royal Academy of Engineering/Siemens Research Chair, and the Head of the Electrical Machines and Drives Research Group, the Academic Director of Sheffield Siemens Wind Power Research Centre, the Director of CRRC Electric Drives Technology Research Centre, and the Director of Midea Electric Machines and Controls Research Centre. His current major research interests include the design and control of permanent magnet brushless machines and drives for applications ranging from automotive to renewable energy. He has received >35 Best Paper Awards, including 6 IEEE Transactions and IET Proceedings Prize Paper Awards. He is a Fellow of Royal Academy of Engineering and a Fellow of Institute of Engineering and Technology (IET), U.K.

**Adam Pride** (M'97) received the B.Sc. and M.Sc. degrees in electrical engineering from the University of Manchester Institute of Science and Technology (now the University of Manchester), Manchester, U.K., in 1977 and 1979, respectively. He was with Froude Consine Ltd., Worcester, U.K., where he worked on research and development of eddy-current dynamometers for automotive engine testing. Since 1995, he has been with the U.K. Research Centre, IMRA Europe SAS, Brighton, U.K., where he has worked on a wide range of motors and actuators for automotive applications. He has co-authored 28 academic papers and has 19 patents. His particular interests include Halbach magnetized permanent-magnet (PM) machines and analysis of optimum slot/pole combinations for concentrated winding PM machines.

Mr. Pride was awarded with a Silver Medal in the Worshipful Company of Turners/IMechE 1988 Engineering Design Competition for a fast-response motoring/absorbing dynamometer.

**Rajesh P. Deodhar** (M'89–S'94–SM'01) received the B.Eng. degree from University of Mumbai, India, in 1989, the M.Tech. degree from Centre for Electronics Design and Technology, Indian Institute of Science, Bangalore, India, in 1991, both in electronics engineering, and the Ph.D. degree from University of Glasgow, Scotland, U.K., in 1996.

Dr. Deodhar has a substantial and a global research profile in the field of electric machines and drives. In 1998, he joined IMRA Europe SAS U.K. Research Centre, Brighton, U.K., where he currently serves as Project Manager working on the design and analysis of a wide range of motors and actuators used in automotive components and systems.

Dr. Deodhar has received numerous awards, including the Indian Institute of Science Gold Medal in 1991, the IEEE Industry Applications Society Electric Machines Committee first prize paper Award in 1996, the IEEE Transactions on Industry Applications second prize paper Award in 1998. More recently, he has been a prize paper award recipient at the IEEE international conferences in 2010, 2012 and 2014. He serves as a reviewer for a number of IEEE journals and as a Technical Planning Committee member for a number of international conferences, and, is a past Associate Editor for the IEEE Transactions on Industry Applications. He is a Chartered Engineer and a Fellow of the Institution of Engineering and Technology in the U.K.

Toshinori Sasaki received the B.Sc. degree in mechanical from the University of Okayama, Japan, in 1985. After graduation, he joined Aisin Seiki Co. in Japan, where he has worked in various technical and management roles over past 30 years.

Mr. Sasaki gained additional overseas experience by working at the Aisin Technical Centre of America (ATCA). Since 2014, he has served as the General Manager of IMRA Europe SAS UK Research Centre at Brighton UK, where he oversees the development of advanced far-future automotive technologies.